Contents

Chapter 1

Theory

1.1 Context

1.2 The induced electric field equation

The electromagnetic field generated by the current density flowing through the coil, J_{coil}, and that induced in the plasma, J_{ind}, is governed by the Maxwell's equations

$$\nabla \cdot \boldsymbol{E} = \frac{\rho}{\epsilon_0} \tag{1.1a}$$

$$\nabla \cdot \boldsymbol{B} = 0 \tag{1.1b}$$

$$\nabla \times \boldsymbol{E} = -\frac{\partial \boldsymbol{B}}{\partial t} \tag{1.1c}$$

$$\nabla \times \boldsymbol{B} = \mu_0 \left(\boldsymbol{J_{coil}} + \boldsymbol{J_{ind}} \right) + \epsilon \mu_0 \frac{\partial \boldsymbol{E}}{\partial t} \tag{1.1d}$$

where $\boldsymbol{E}$ and $\boldsymbol{B}$ are the three-dimensional components of the electric and magnetic fields, μ_0 and ϵ_0 the permeability and permittivity of the free space and ρ the charge density. The charge density ρ is supposed null because the excitation frequency is by far smaller than the fundamental frequency of the plasma, which leads to a quasi-neutral state of the plasma. Furthermore the displacement current can also be neglected, which is done by splitting the electric field E into the induced electric field E_{ind} and the electric field generated by the coils E_{coils}. The term $\epsilon \mu_0 \partial E_{ind} / \partial t$ is removed by neglecting the electromagnetic waves and the term $\epsilon \mu_0 \partial E_{coil} / \partial t$ is removed by neglecting the electric oscillations. The Maxwell's equations boil down to

$$\nabla \cdot \boldsymbol{E} = 0 \tag{1.2a}$$

$$\nabla \cdot \boldsymbol{B} = 0 \tag{1.2b}$$

$$\nabla \times \boldsymbol{E} = -\frac{\partial \boldsymbol{B}}{\partial t} \tag{1.2c}$$

$$\nabla \times \boldsymbol{B} = \mu_0 \left(\boldsymbol{J_{coil}} + \boldsymbol{J_{ind}} \right) \tag{1.2d}$$

It is convenient to introduce the magnetic vector potential $\boldsymbol{A}$

$$\boldsymbol{B} = \nabla \times \boldsymbol{A} \tag{1.3}$$

which, introduced in the Maxwell's equations, lead to

$$\boldsymbol{E} = -\frac{\partial \boldsymbol{A}}{\partial t} \tag{1.4a}$$

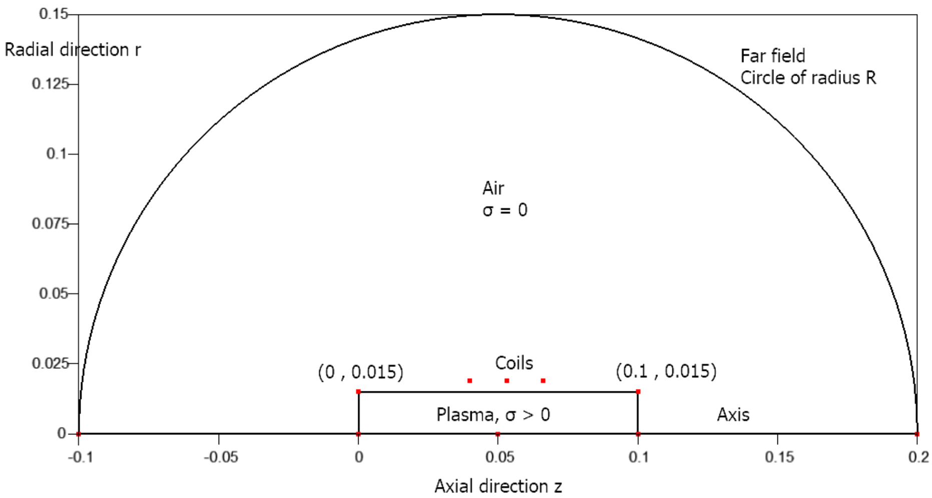

Figure 1.1: Geometry of the inductively coupled plasma torch and its external domain.

$$\nabla^2 \boldsymbol{A} = -\mu_0 \left(\boldsymbol{J_{coil}} + \boldsymbol{J_{ind}} \right) \tag{1.4b}$$

The induced current density is expressed by the simplified Ohm's law

$$\boldsymbol{J_{ind}} = \sigma \boldsymbol{E} = -\sigma \frac{\partial \boldsymbol{A}}{\partial t} \tag{1.5}$$

Further simplifications are made by assuming a sinusoidal time variation with frequency f. The classical complex notation is then used to eliminate the time variable from Eq. (1.4b). To do so let us define

$$\boldsymbol{J_{coil}}(\boldsymbol{r}, t) = \Re \left\{ \widetilde{\boldsymbol{J}}_{\boldsymbol{coil}}(\boldsymbol{r}) e^{i\omega t} \right\} \tag{1.6a}$$

$$\boldsymbol{A}(\boldsymbol{r}, t) = \Re \left\{ \widetilde{\boldsymbol{A}}(\boldsymbol{r}) e^{i\omega t} \right\} \tag{1.6b}$$

with $\widetilde{\boldsymbol{J}}_{\boldsymbol{coil}}$ and $\widetilde{\boldsymbol{A}}$ the phasors and $\omega = 2\pi f$. One then gets

$$\nabla^2 \widetilde{\boldsymbol{A}} - i\mu_0 \sigma \omega \widetilde{\boldsymbol{A}} = -\mu_0 \widetilde{\boldsymbol{J}}_{\boldsymbol{coil}} \tag{1.7}$$

Under the assumption of an axisymmetric configuration for the induction circuit, the electric current density flowing in the coil and, consequently, the magnetic vector potential will only have tangential components. The electric current density $\widetilde{\boldsymbol{J}}_{\boldsymbol{coil}}$ is purely real so that

$$\widetilde{\boldsymbol{J}}_{\boldsymbol{coil}} = J_{coil} \overline{\boldsymbol{e}}_\theta \tag{1.8a}$$

$$\widetilde{\boldsymbol{A}} = \left(A_\theta^r + i A_\theta^i \right) \overline{\boldsymbol{e}}_\theta \tag{1.8b}$$

$$\widetilde{\boldsymbol{E}} = \left(E_\theta^r + i E_\theta^i \right) \overline{\boldsymbol{e}}_\theta = \omega \left(A_\theta^i - i A_\theta^r \right) \overline{\boldsymbol{e}}_\theta \tag{1.8c}$$

Equation (1.7) can then be expressed in terms of electric field and be split into the followings

$$\frac{1}{r} \frac{\partial}{\partial r} \left(r \frac{\partial E_\theta^r}{\partial r} \right) + \frac{\partial^2 E_\theta^r}{\partial z^2} - \frac{E_\theta^r}{r^2} + \mu_0 \sigma \omega E_\theta^i = 0 \tag{1.9a}$$

$$\frac{1}{r} \frac{\partial}{\partial r} \left(r \frac{\partial E_\theta^i}{\partial r} \right) + \frac{\partial^2 E_\theta^i}{\partial z^2} - \frac{E_\theta^i}{r^2} - \mu_0 \sigma \omega E_\theta^r = \mu_0 \omega J_{coil} \tag{1.9b}$$

Provided that J_{coil} is known, equations (1.9a)- (1.9b) can be solved to calculate the induced electric field. The magnetic field can then be retrieved through Eq. (1.2c)

$$B_z = B_{zr} + iB_{zi} = \frac{1}{i\omega}\frac{\partial(E_\theta^r + iE_\theta^i)}{\partial z} = \frac{1}{\omega}\frac{\partial(E_\theta^i - iE_\theta^r)}{\partial z} \tag{1.10a}$$

$$B_r = B_{rr} + iB_{ri} = -\frac{1}{i\omega}\frac{1}{r}\frac{\partial r(E_\theta^r + iE_\theta^i)}{\partial r} = \frac{1}{\omega}\frac{1}{r}\frac{\partial r(-E_\theta^i + iE_\theta^r)}{\partial r} \tag{1.10b}$$

If an electric current $I_{coil} = J_{coil}\Omega_{coil}$ flows through the coils of section Ω_{coil}, then one can explicit the right-hand side of Eq. (1.9b). The outer inductor is approximated by a series of n_r parallel rings of radius R_i and axial position Z_i

$$J_{coil}(z,r) = \sigma E_{coil}(z,r) = -i\omega\sigma A_{coil}(z,r) = -i\omega\sigma\frac{\mu_0 I_c}{2\pi}\sum_{i=1}^{n_r}\sqrt{\frac{R_i}{r}}G(m) \tag{1.11a}$$

$$G(m) = \frac{(2-m)K(m) - 2E(m)}{\sqrt{m}} \tag{1.11b}$$

$$m = \frac{4rR_i}{(r+R_i)^2 + (Z_i - z)^2} \tag{1.11c}$$

with $K(m)$ and $E(m)$ being the elliptic integrals of first and second kind, respectively.

1.3 Boundary conditions

The induced electric field must satisfy boundary conditions so that the system of equations built by the numerical method can be solved. On the axis, because of the axisymmetric hypothesis, the vanishing condition is imposed

$$E_\theta(z,0) = 0 \tag{1.12}$$

Two approaches exist in terms of type of computational domain and associated boundary conditions. A first common configuration computes the electric field inside the torch only. This approach, introduced by McKelliget [1], solves the induction equations (1.9) inside the torch, each element inside the torch being considered as an infinitely thin current-carrying loop. The electric field on the boundary of the torch is obtained by summing up all the contributions coming from both excitation and induced currents flowing in the coil and in the plasma, respectively. Although mathematically elegant, this integral boundary procedure is computationally expensive, as it couples every boundary cell to all interior cells. Moreover, due to the term accounting for the effects of the induced currents, the whole distribution of E_θ in the plasma region needs to be known to determine the vector potential at each point on the boundaries. Thus, an iterative approach has to be employed to solve the electromagnetic field equations, leading to slow convergence of the numerical process. This approach will not be implemented in this project.

Another approach uses a computational grid which extends well outside the plasma discharge region, so that simpler boundary conditions can be adopted for the electric field. Vanden Abeele [2] and Lopes [3] rely on a sufficiently large enough external domain to impose the vanishing conditions

$$E_\theta(z,r) = 0 \qquad \text{if the external domain is large enough} \tag{1.13}$$

Bernardi *et al.* [4] introduced a new concept that allows the external domain to be considerably smaller without affecting the quality of the solution. The border of the external domain have been placed far enough from the plasma region in order to use boundary conditions for the electric field as if the torch were a magnetic dipole produced by the electric current flowing in the plasma and in the induction coil. Far enough away from the discharge, the whole system can be treated as a single magnetic dipole placed at the mid-coil point, with momentum parallel to the axis of the torch. Under such an assumption and taking a cylindrical (z, r) reference frame with the origin at the dipole and z-axis parallel to its momentum, the electric field at sufficient distance from the torch is given by the classic expression:

$$E_\theta(z, r) = C\frac{r}{(r^2 + z^2)^{(3/2)}} \tag{1.14}$$

In the later relation, C is a constant which accounts for the momentum of the dipole, whose value is not known *a priori* as it depends upon the induced currents which, in turn, depend upon the electric field in the discharge region. However, the value of C is not actually required for our purposes. By taking the $z-$ and $r-$derivatives of Eq. (1.14) and eliminating the unknown constant C, one obtains boundary conditions to be applied on the external domain:

$$\frac{\partial E_\theta}{\partial z} = -\frac{3z}{r^2 + z^2}E_\theta \tag{1.15a}$$

$$\frac{\partial E_\theta}{\partial r} = \frac{1 - 3r^2(r^2 + z^2)^{-1}}{r}E_\theta \tag{1.15b}$$

1.4 Skin effect

According to Lenz's law, the currents in the plasma produce a magnetic field to counteract the electromagnetic field of the induction coil. This gives rise to a limitation of the penetration depth of the external magnetic field. This so-called skin-depth δ depends on the electrical conductivity σ and the excitation frequency f

$$\delta = \sqrt{\frac{1}{\pi f \mu_0 \sigma}} \tag{1.16}$$

The higher the electrical conductivity of the plasma and the higher the resonant frequency, the lower the skin-depth, and thus, the penetration of the external electromagnetical field into the plasma. This defines the tendency for alternating current (AC) signals to flow near the outer edge of the electrical conductor. The electric current takes the form

$$J(z, t) = J_0 e^{-z/\delta} \cos(\omega t - z/\delta) \tag{1.17}$$

with z the radial coordinate starting from the wall of the torch.

Chapter 2

Numerical discretization

2.1 Finite element method

2.1.1 General considerations

The finite element (FE) method introduces the concept representation of the solution by functions. The spatial domain is discretized into elements of chosen shapes (triangles, quadrangles, etc.) and equations (1.9a) and (1.9b) are solved at the corners of these elements. The solution can be interpolated inside the elements through shape functions $N_j(r, z)$, for which the order will fix the precision of the result. The solution at any point in the two-dimensional space is then based on the knowledge of the solution E_j at the corners of the elements:

$$E(z, r) = \sum_k N_k(z, r) E_k \tag{2.1}$$

The numerical discretization of the physical equations does not allow the strict respect of the left-hand side being equal to the right-hand side. A residual is introduced in the physical equations. The FE method is based on the weighted minimalisation of the residual over the whole domain. In order to defined the discretized equation at node j, the Galerkin FE method picks the shape function at that node $N_j(z, r)$ as the weight factor:

$$2\pi \int_\Omega r N_j(z, r) \left(\nabla^2 \widetilde{\boldsymbol{E}}_j - i\mu_0\sigma\omega\widetilde{\boldsymbol{E}}_j - i\mu_0\omega\widetilde{\boldsymbol{J}}_{\boldsymbol{coil}j} \right) drdz = 0 \tag{2.2}$$

The shape functions are null everywhere except at the node j of interest. The choice of the Galerkin method has the consequence that only the direct neighbour nodes k are involved in the discretized equations at node j. These shape functions are moreover of order one because no special physical behaviour is expected.

2.1.2 Galerkin finite element equations

Assuming an implicit summation over the index k, one can write down the Galerkin FE discretization of equations (1.9a) and (1.9b) at node j as

$$\int_\Omega r N_j \left(\frac{1}{r}\frac{\partial}{\partial r}\left(r \frac{\partial N_k}{\partial r} \right) E^r_{\theta k} + \frac{\partial^2 N_k}{\partial z^2} E^r_{\theta k} - \frac{N_k E^r_{\theta k}}{r^2} + \mu_0\sigma\omega N_k E^i_{\theta k} \right) drdz = 0 \tag{2.3a}$$

$$\int_\Omega r N_j \left(\frac{1}{r}\frac{\partial}{\partial r}\left(r \frac{\partial N_k}{\partial r} \right) E^i_{\theta k} + \frac{\partial^2 N_k}{\partial z^2} E^i_{\theta k} - \frac{N_k E^i_{\theta k}}{r^2} - \mu_0\sigma\omega N_k E^r_{\theta k} - \mu_0\omega J_{coil} \right) drdz = 0 \tag{2.3b}$$

Integrating by part the two first terms of each equation allows the usage of shape functions of first order:

$$\int_\Omega \left(-r\frac{\partial N_j}{\partial r}\frac{\partial N_k}{\partial r}E^r_{\theta k} - r\frac{\partial N_j}{\partial z}\frac{\partial N_k}{\partial z}E^r_{\theta k} - \frac{N_j N_k E^r_{\theta k}}{r} + \mu_0\sigma\omega r N_j N_k E^i_{\theta k} \right) drdz \\ + \underbrace{\int_{\partial\Omega} \left(rN_j n_r \frac{\partial E^r_\theta}{\partial r} + rN_j n_z \frac{\partial E^r_\theta}{\partial z} \right) d\Gamma}_{=\int_{\partial\Omega} rN_j \frac{\partial E^r_\theta}{\partial n} d\Gamma \text{ far field condition}} = 0 \tag{2.4a}$$

$$\int_\Omega \left(-r\frac{\partial N_j}{\partial r}\frac{\partial N_k}{\partial r}E^i_{\theta k} - r\frac{\partial N_j}{\partial z}\frac{\partial N_k}{\partial z}E^i_{\theta k} - \frac{N_j N_k E^i_{\theta k}}{r} - \mu_0\sigma\omega r N_j N_k E^r_{\theta k} - \mu_0 \omega r N_j J_{coil} \right) drdz \\ + \underbrace{\int_{\partial\Omega} \left(rN_j n_r \frac{\partial E^i_\theta}{\partial r} + rN_j n_z \frac{\partial E^i_\theta}{\partial z} \right) d\Gamma}_{=\int_{\partial\Omega} rN_j \frac{\partial E^i_\theta}{\partial n} d\Gamma \text{ far field condition}} = 0 \tag{2.4b}$$

Note that the boundary integrals make appear the $z-$ and $r-$ derivatives of the electric field, which were specified in Eqs. (1.15). Taking into account that information, the boundary integral for the real component (and similarly for the imaginary one) becomes

$$\int_{\partial\Omega} rN_j \frac{\partial E^r_\theta}{\partial n} d\Gamma = \int_{\partial\Omega} N_j N_k \left(n_r \frac{(z-z_c)^2 - 2r^2}{r^2 + (z-z_c)^2} - 3n_z \frac{r(z-z_c)}{r^2+(z-z_c)^2} \right) E^r_{\theta k} d\Gamma \tag{2.5}$$

where z_c is the axial location of the mid-coil point. For the sake of clarity, let us define the following elemental matrices

$$m_{jk} = \int_\Omega r N_j N_k drdz \tag{2.6a}$$

$$k_{jk} = -\int_\Omega r \left(\frac{\partial N_j}{\partial r}\frac{\partial N_k}{\partial r} + \frac{\partial N_j}{\partial z}\frac{\partial N_k}{\partial z} \right) drdz \tag{2.6b}$$

$$p_{jk} = -\int_\Omega \frac{N_j N_k}{r} drdz \tag{2.6c}$$

$$s_{jk} = \int_{\partial\Omega} N_j N_k \left(n_r \frac{(z-z_c)^2 - 2r^2}{r^2+(z-z_c)^2} - 3n_z \frac{r(z-z_c)}{r^2+(z-z_c)^2} \right) d\Gamma \tag{2.6d}$$

These matrices are dependent on the shape functions only and can be evaluated through analytical expressions for some of them, or through numerical quadratures for others. Let us also use the same paradigm for the forcing term J_{coil} as for the unknown induced electric field: $J_{coil}(z,r) = \sum_k N_k(z,r) J_{coil,k}$. This allows the Galerkin FE to boil down to

$$(k_{jk} + p_{jk} + s_{jk}) E^r_{\theta k} + \mu_0\sigma\omega m_{jk} E^i_{\theta k} = 0 \tag{2.7a}$$

$$(k_{jk} + p_{jk} + s_{jk}) E^i_{\theta k} - \mu_0\sigma\omega m_{jk} E^r_{\theta k} = \mu_0\omega m_{jk} J_{coil,k} \tag{2.7b}$$

or in terms of matrix representation

$$\begin{pmatrix} k_{jk}+p_{jk}+s_{jk} & \mu_0\sigma\omega m_{jk} \\ -\mu_0\sigma\omega m_{jk} & k_{jk}+p_{jk}+s_{jk} \end{pmatrix} \begin{pmatrix} E^r_{\theta k} \\ E^i_{\theta k} \end{pmatrix} = \begin{pmatrix} 0 \\ \mu_0\omega m_{jk} J_{coil,k} \end{pmatrix} \tag{2.8}$$

The real and imaginary components are coupled through the term m_{jk}. In the case where the electrical conductivity σ of the medium is null, then only the imaginary component of the induced electric field is non-zero.

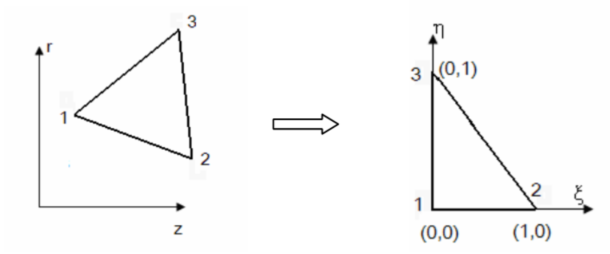

Figure 2.1: Definition of the triangular FE and its transformation to the (ξ, η) plane.

2.1.3 Elemental matrices for triangular elements

The analytical evaluation of the elemental matrices m_{jk} and k_{jk} is more easily performed in a new (η, ξ) plane defined in Fig. 2.1. Doing so the linear shape functions take the form

$$N_1(\eta, \xi) = 1 - \eta - \xi \tag{2.9a}$$
$$N_2(\eta, \xi) = \eta \tag{2.9b}$$
$$N_3(\eta, \xi) = \xi \tag{2.9c}$$

The integrals on this right triangle in (ξ, η) plane are related to the integrals on the true element (of area Ω) in the (z, r) plane by the Jacobian of the transformation which apply the element on the right triangle

$$\int_\Omega \psi(z, r) dr dz = \int_0^1 \int_0^{1-\xi} \psi(\eta, \xi) |J(\xi, \eta)| d\eta d\xi \tag{2.10}$$

where $|J(\xi, \eta)|$ is the determinant of the Jacobian defined as

$$J(\eta, \xi) = \begin{pmatrix} \frac{\partial r}{\partial \xi} & \frac{\partial r}{\partial \eta} \\ \frac{\partial z}{\partial \xi} & \frac{\partial z}{\partial \eta} \end{pmatrix} \tag{2.11}$$

By choosing $\psi = 1$ one gets the relation $|J(\xi, \eta)| = 2\Omega$ which is easily computed. Let us define the normals of the segment on the other side of a node:

$$\boldsymbol{n}_1 = (r_3 - r_2)\overline{\boldsymbol{e}}_z + (z_2 - z_3)\overline{\boldsymbol{e}}_r \tag{2.12a}$$
$$\boldsymbol{n}_2 = (r_1 - r_3)\overline{\boldsymbol{e}}_z + (z_3 - z_1)\overline{\boldsymbol{e}}_r \tag{2.12b}$$
$$\boldsymbol{n}_3 = (r_2 - r_1)\overline{\boldsymbol{e}}_z + (z_1 - z_2)\overline{\boldsymbol{e}}_r \tag{2.12c}$$

Then the analytical expressions for the elemental matrices m_{jk} and k_{jk} are (see Detandt [5])

$$m_{jk} = \frac{\Omega(r_1 + r_2 + r_3 + r_j + r_k)(1 + \delta_{jk})}{60} \tag{2.13a}$$
$$k_{jk} = -\frac{(r_1 + r_2 + r_3)(n_j^r n_k^r + n_j^z n_k^z)}{12\Omega} \tag{2.13b}$$

The elemental matrix p_{jk} requires a numerical quadrature because of the difficulty to evaluate analytically. For this purpose, four internal quadrature points are taken in order to avoid any singularity at $r = 0$ (see Table 2.1):

$$p_{jk} = -\int_\Omega \frac{N_j N_k}{r} dr dz = -\sum_{n=1}^{4} w_n \frac{N_j(\eta_n, \xi_n) N_k(\eta_n, \xi_n)}{r_n} |J(\xi, \eta)| \tag{2.14}$$

n	ξ	η	w	N_1	N_2	N_3	r
1	$1/3$	$1/3$	-27/96	$1/3$	$1/3$	$1/3$	$(r_1 + r_2 + r_3)/3$
2	0.2	0.6	$25/96$	0.2	0.2	0.6	$0.2(r_1 + r_2) + 0.6r_3$
3	0.6	0.2	$25/96$	0.2	0.6	0.2	$0.2(r_1 + r_3) + 0.6r_2$
4	0.2	0.2	$25/96$	0.6	0.2	0.2	$0.2(r_2 + r_3) + 0.6r_1$

Table 2.1: Quadrature table for the element matrix p_{jk}.

d	ξ	w
1 and 2	$\pm$ 0.8611363116	0.3478548451
3 and 4	$\pm$ 0.3399810436	0.6521451548

Table 2.2: Quadrature table for the element matrix s_{jk}.

2.1.4 Elemental matrices for edge elements

The boundary integral s_{jk} in Eq. (2.6) appears only on the nodes lying on the boundary of the external domain. The shape functions N_j and N_k are linear and (n_z, n_r) is the normal to the edge element, pointing outwards the domain. This elemental matrix is not simple and a numerical quadrature must be performed to compute it. To perform this numerical quadrature, the two nodes at (z_1, r_1) and (z_2, r_2) that define the edge element must be transformed to a new coordinate $-1 \leq \xi \leq 1$ through the relation

$$z = z_1 + \frac{\xi + 1}{2}(z_2 - z_1) \tag{2.15a}$$

$$r = r_1 + \frac{\xi + 1}{2}(r_2 - r_1) \tag{2.15b}$$

The shape functions at the two nodes are then given by

$$N_1(\xi) = \frac{1 - \xi}{2} \tag{2.16a}$$

$$N_2(\xi) = \frac{1 + \xi}{2} \tag{2.16b}$$

and the quadrature is approximated by

$$s_{jk} = \sum_{d=1}^{4} w_d N_j(\xi_d) N_k(\xi_d) \left(n_r \frac{(z_d - z_c)^2 - 2r_d^2}{r_d^2 + (z_d - z_c)^2} - 3n_z \frac{r(z_d - z_c)}{r_d^2 + (z_d - z_c)^2} \right) \frac{L}{2} \tag{2.17}$$

with $L = \sqrt{(z_2 - z_1)^2 + (r_2 - r_1)^2}$ being the length of the edge element and the quadrature points ξ_d and weights w_d are defined in Table 2.2.

Chapter 3

Numerical results

This chapter displays the results of the resolution of Equations (2.8) inside and around an inductively coupled plasma torch. The geometry of the whole domain and detail of the VKI minitorch are shown in Fig. 3.1. This minitorch has a diameter of $3cm$, an excitation frequency of 27MHz and works with argon. The following sections will study

- the influence of the type of boundary condition set at the far field,
- the influence of the radius R of the external domain,
- the convergence rate of the numerical method as a function of degrees of freedom inside the torch,
- the influence of the electrical conductivity σ on the solution,
- the influence of the excitation frequency f of the coils

3.1 Influence of the boundary condition set on the external domain

This section studies the impact of the boundary condition set on the external domain. As explained in Section 1.3, two boundary conditions can be set, the vanishing one $E_\theta = 0$ for

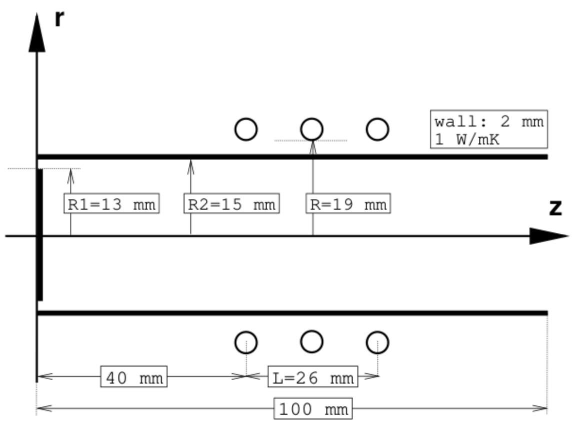

Figure 3.1: Geometry of the VKI minitorch (vanden Abeele [2]).

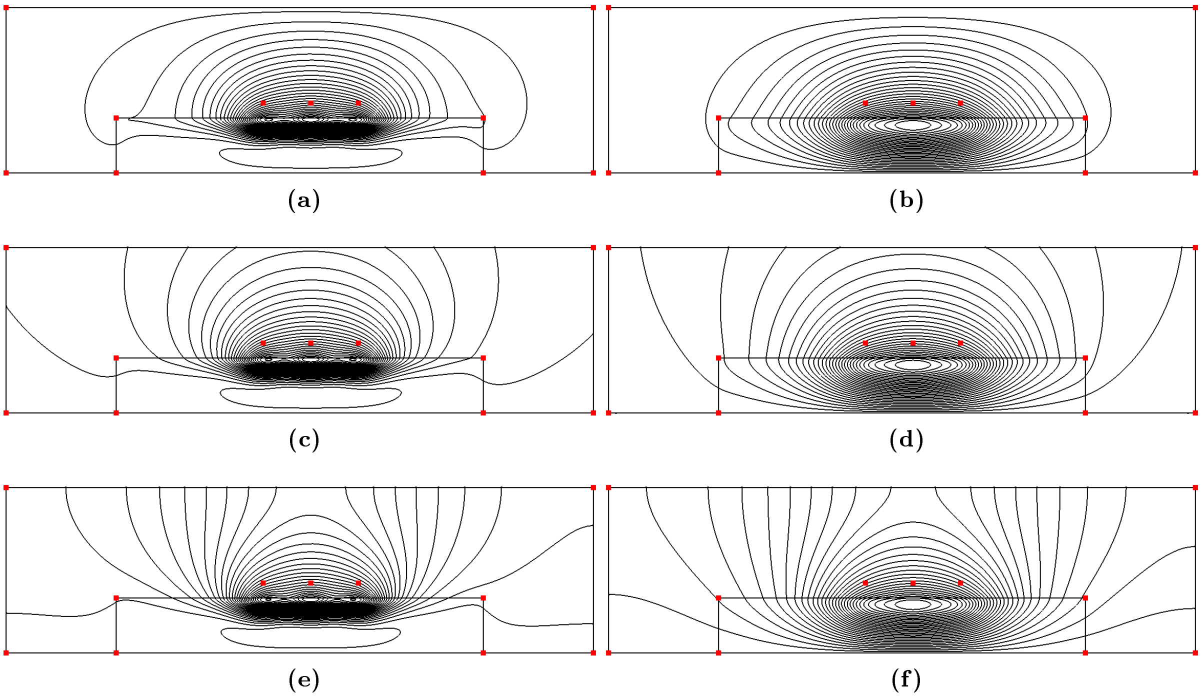

Figure 3.2: Influence of the boundary condition set on the external domain. Curves of isovalues of the (left) real part and (right) imaginary part of the induced electric field. (top) $E_\theta = 0$, (middle) $\partial E_\theta/\partial n$ and (bottom) $\partial E_\theta/\partial n = 0$ is set on the far field.

sufficiently large domains; and the specification of $\partial E_\theta/\partial n$ for domains of smaller size. The outer domain consists here in a rectangle whose sides are offset by a distance R from each of the three sides of the torch. A large domain ($R = 1m$) will be used as a reference for computations with a small external domain ($R = 0.005m$). The additional boundary condition $\partial E_\theta/\partial n = 0$ is also tested and is equivalent to cancelling the boundary integrals in Eqs (2.4).

Figures 3.2, 3.3 and 3.4 show the influence of the boundary condition set on the external domain on the induced electric field. Figure 3.2 shows curves of isovalues of the electric field when $E_\theta = 0$, $\partial E_\theta/\partial n$ or $\partial E_\theta/\partial n = 0$ are imposed. In the case of $E_\theta = 0$, the forced containment of the electric field is clearly put forward. The case $\partial E_\theta/\partial n = 0$ also fails to predict the correct electric field on the outer edge. Figures 3.3 and 3.4 show cuts along the radial and axial directions, at the middle coil $z = 0.053m$ and on the wall of the torch $z = 0.015m$ respectively. Only the imposition of $\partial E_\theta/\partial n$ on the boundary leads to the best matching results in comparison with a large external domain. The condition $E_\theta = 0$ displays non-physical behaviours at the left and right sides of the torch for $\sigma \geq 1000S/m$. The worst prediction with $\partial E_\theta/\partial n$ is along the wall of the torch at low values of the electrical conductivity, for the imaginary part of E_θ.

3.2 Influence of the size of the external domain

This section studies the impact of the size of the external domain. The outer domain consists here in a rectangle whose sides are offset by a distance R from each of the three sides of the torch. A large domain ($R = 1m$) will be used as a reference, the distance being increased from $R = 0.005m$ to $1m$. The additional boundary condition $\partial E_\theta/\partial n = 0$ is also tested and is equivalent to cancelling the boundary integrals in Eqs (2.4). Three values of the electrical conductivity are taken ($\sigma = 10^2$, 10^3 and $10^4 S/m$) and the excitation frequency is set to 27MHz.

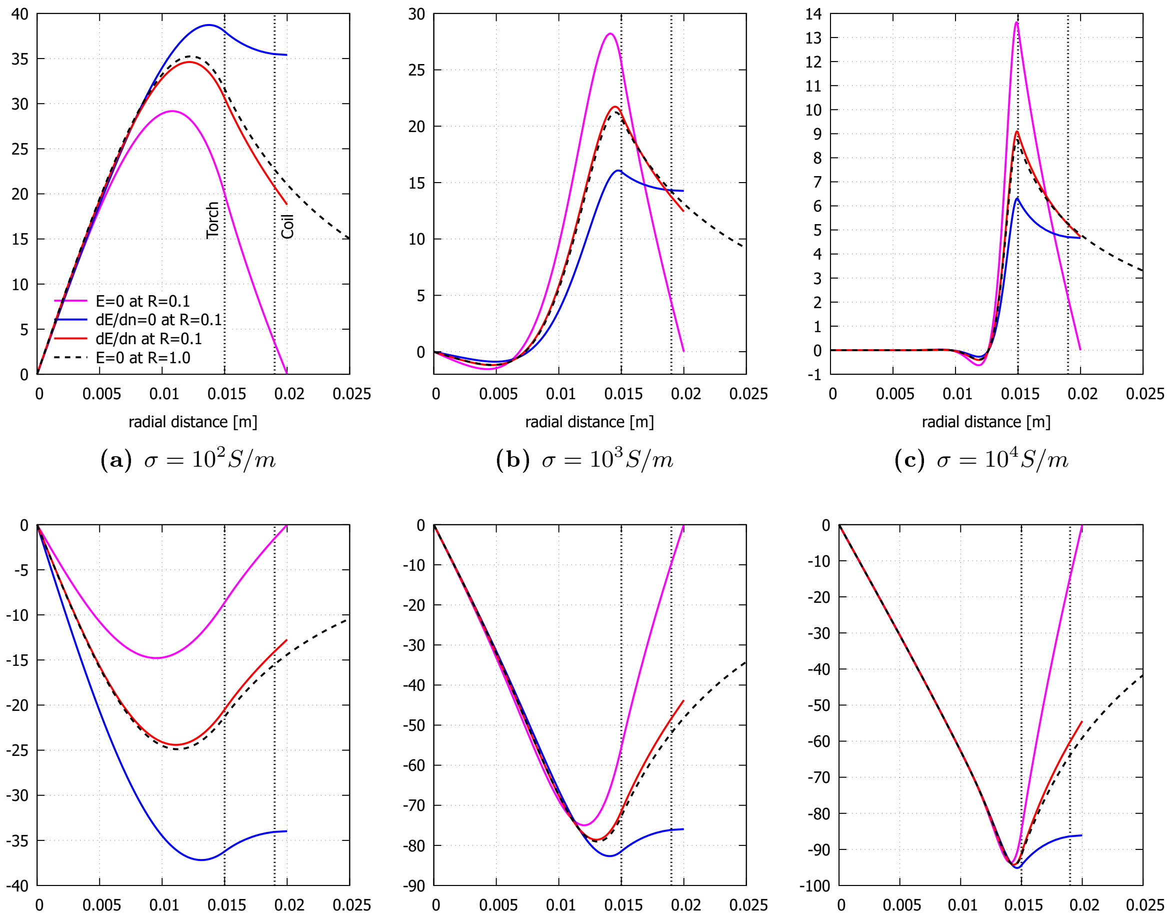

(a) $\sigma = 10^2 S/m$ **(b)** $\sigma = 10^3 S/m$ **(c)** $\sigma = 10^4 S/m$

(d) $\sigma = 10^2 S/m$ **(e)** $\sigma = 10^3 S/m$ **(f)** $\sigma = 10^4 S/m$

Figure 3.3: Influence of the boundary condition set on the external domain. Radial cut located at the middle coil ($z = 0.053m$). (top) Real part and (bottom) imaginary part of the induced electric field for three values of the electrical conductivity σ.

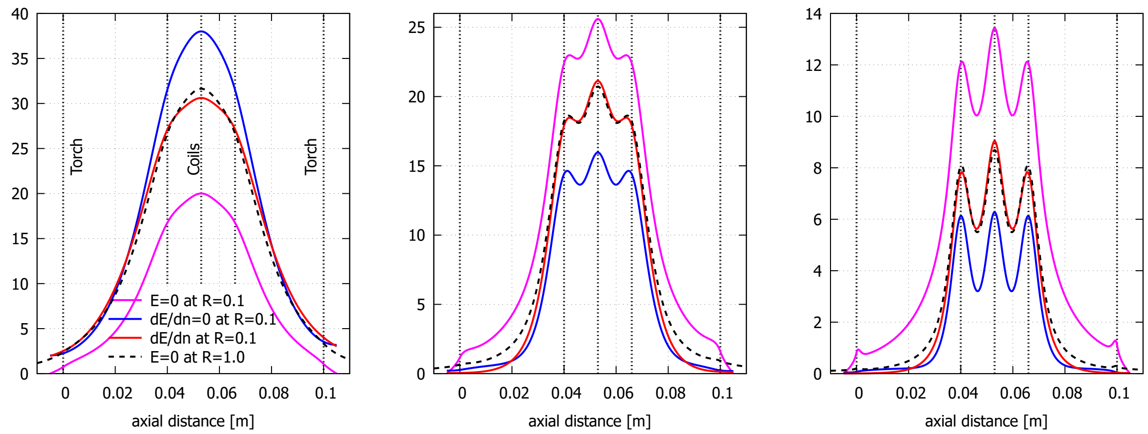

(a) $\sigma = 10^2 S/m$ **(b)** $\sigma = 10^3 S/m$ **(c)** $\sigma = 10^4 S/m$

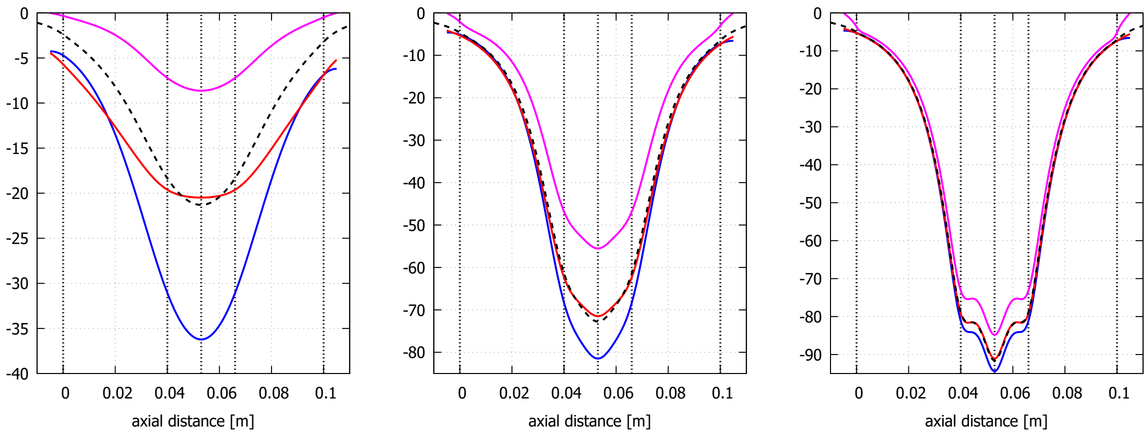

(d) $\sigma = 10^2 S/m$ **(e)** $\sigma = 10^3 S/m$ **(f)** $\sigma = 10^4 S/m$

Figure 3.4: Influence of the boundary condition set on the external domain. Axial cut located on the torch ($r = 0.015m$). (top) Real part and (bottom) imaginary part of the induced electric field for three values of the electrical conductivity σ.

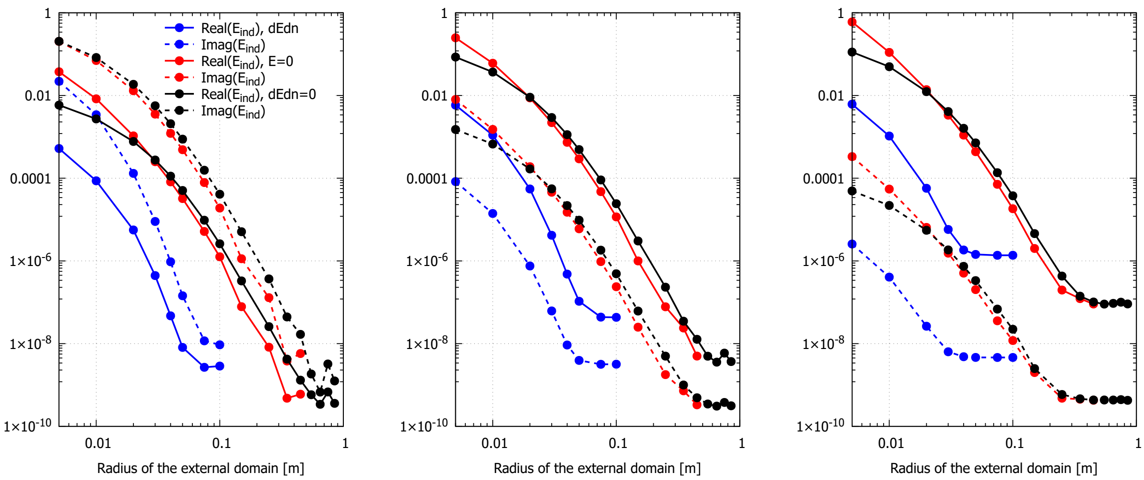

(a) $\sigma = 10^2 S/m$ **(b)** $\sigma = 10^3 S/m$ **(c)** $\sigma = 10^4 S/m$

Figure 3.5: Influence of the size of the external domain on the solution. Relative error accumulated on the inside of the torch.

To measure the impact of the size of the external domain, the relative error for both real and imaginary parts of the electric field is defined as

$$\epsilon_{rel} = \sqrt{\frac{\sum_m (E_m - E_m^{R=1})^2}{\sum_m (E_m^{R=1})^2}} \tag{3.1}$$

where the index m runs for all the nodes inside the torch (and on its wall) and $E^{R=1}$ is the reference solution computed with $R = 1m$. Figure 3.5 shows the relative error for the three boundary conditions at the outer edge, as a function of the distance R. Among all boundary conditions set on the external domain, the imposition of $\partial E_\theta / \partial n$ displays the fastest convergence. It requires a distance $R = 0.075m$ for $\sigma = 10^2 S/m$ and a distance $R = 0.04m$ for $\sigma = 10^4 S/m$. The two other boundary conditions require at least $R = 0.4m$ before convergence. From now on it is supposed that the condition $\partial E_\theta / \partial n$ is imposed on the outer edge as it displays the best behaviour.

3.3 Convergence rate

This section studies the convergence rate of the Galerkin finite element method by increasing the number of nodes inside the torch. The torch is meshed uniformly by right-angled triangles of identical leg size. The size of the external domain is chosen sufficiently big, see Section 3.2. The proof of convergence is based on the relative error from Eq. (3.1) where this time the reference field is the solution on the finest mesh. The results are shown in Fig. 3.6 for three values of the electrical conductivity. It appears that the Galerkin finite element method based on linear triangular elements has a convergence rate of -2.

3.4 Influence of the electrical conductivity

This section studies the impact of an increase in the electrical conductivity σ on the solution. The immediate impact of such an increase is the decrease of the skin-depth of the total electric field, as explained in Section 1.4. Figure 3.7 shows the real and imaginary parts of the induced and

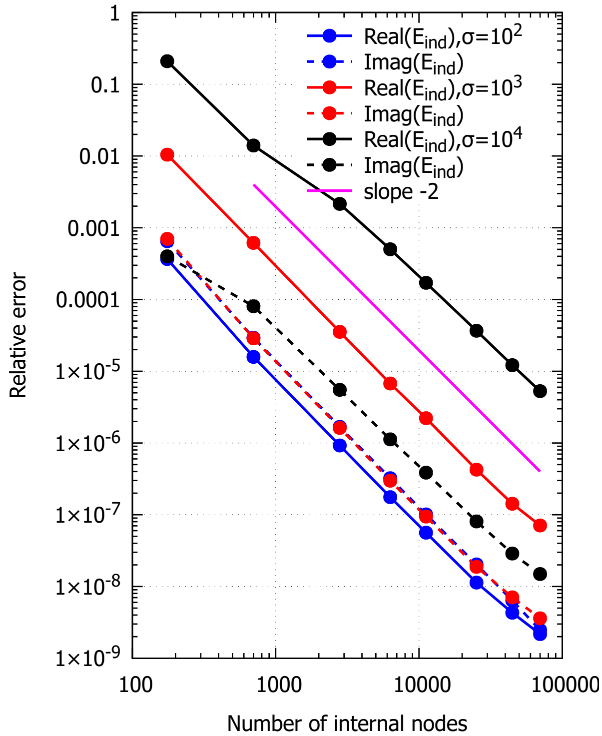

Figure 3.6: Convergence rate

σ	Theoretical δ	Numerical δ
$10^2 S/m$	$9.58mm$	$8.54mm$
$10^3 S/m$	$3.03mm$	$3.07mm$
$10^4 S/m$	$0.96mm$	$0.97mm$

Table 3.1: Theoretical and numerically computed skin-depths as a function of the electrical conductivity.

total electric fields as well as the purely imaginary contribution from the coils. The calculation of the skin-depth is based on the norm of the total electric field

$$\|E_{tot}\| = \sqrt{\left(E_\theta^r\right)^2 + \left(E_\theta^i + E_{coil}\right)^2} \tag{3.2}$$

For an excitation frequency $f = 27.6MHz$, the theoretical skin-depth from Eq. (1.16) and the numerically computed ones are given in Table 3.1. A pretty good agreement emerges, especially for high values of σ.

3.5 Influence of the excitation frequency

This section studies the impact of an increase in the excitation frequency f on the solution. The immediate impact of such an increase is the decrease of the skin-depth of the total electric field, as explained in Section 1.4. Figure 3.7 shows the real and imaginary parts of the induced and total electric fields as well as the purely imaginary contribution from the coils. Note that contrary to the previous section, the amplitude of the forcing term is directly proportional to ω (see Eq (1.11a)), which explains the linear variation of the amplitude of E_{coil} as f increases.

The calculation of the skin-depth is based on the norm of the total electric field

$$\|E_{tot}\| = \sqrt{\left(E_\theta^r\right)^2 + \left(E_\theta^i + E_{coil}\right)^2} \tag{3.3}$$

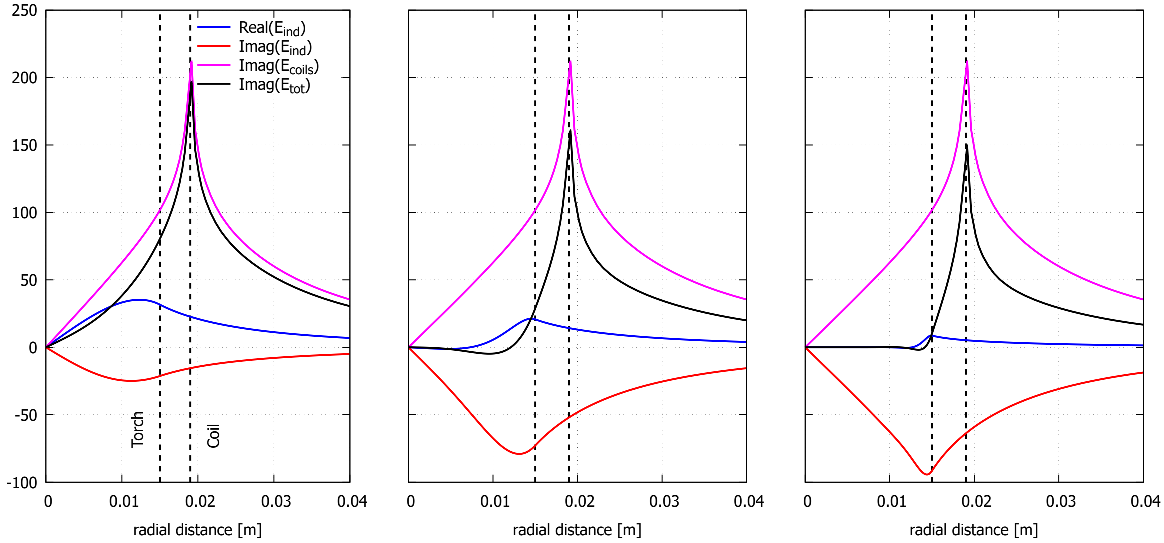

(a) $\sigma = 10^2 S/m$ **(b)** $\sigma = 10^3 S/m$ **(c)** $\sigma = 10^4 S/m$

Figure 3.7: Influence of the electrical conductivity σ on the solution. Cut at $z = 0.053m$ located at the middle coil.

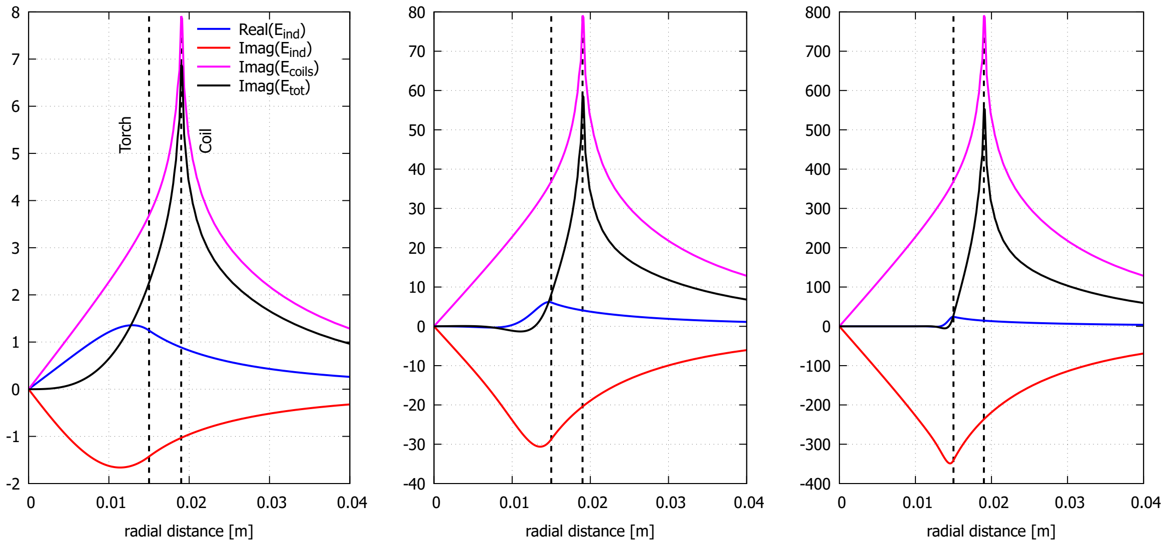

(a) $f = 1MHz$ **(b)** $f = 10MHz$ **(c)** $f = 100MHz$

Figure 3.8: Influence of the excitation frequency f on the solution. Cut at $z = 0.053m$ located at the middle coil.

f	Theoretical δ	Numerical δ
$1MHz$	$7.12mm$	$7.79mm$
$10MHz$	$2.25mm$	$2.26mm$
$100MHz$	$0.71mm$	$0.72mm$

Table 3.2: Theoretical and numerically computed skin-depths as a function of the excitation frequency.

For an electrical conductivity $\sigma = 5000S/m$, the theoretical skin-depth from Eq. (1.16) and the numerically computed ones are given in Table 3.2. A pretty good agreement emerges, especially for high values of f.

Bibliography

[1] J.W. McKelliget. A mathematical model of an inductive plasma torch. Technical Report 86-112.1, University of Lowell, College of Engineering, September 1986.

[2] David vanden Abeele. *An efficient computational model for inductively coupledair plasma flows under thermal and chemical non-equilibrium - with application to atmospheric re-entry flow studies.* PhD thesis, Katholieke Universiteit Leuven, 2000.

[3] Silvânia Lopes. *Integrated CFD Model for Nanoparticle Production in Inductively Coupled Plasma Reactors: Implementation and Application.* PhD thesis, Université Libres de Bruxelles, 2016.

[4] D. Bernardi, V. Colombo, G. G. M. Coppa, and A. D'Angola. Simulation of the ignition transient in rf inductively-coupled plasma torches. *The European Physical Journal D - Atomic, Molecular, Optical and Plasma Physics*, 14(3):337–348, 2001.

[5] Yves Detandt. *Extension of Spectral/Finite Element solver for Large Eddy Simulation (SFE-LES) for axisymmetric bodies.* PhD thesis, Université Libres de Bruxelles, 2004.